Lab on a Chip

PAPER

View Article Online
View Journal | View Issue

Cite this: *Lab Chip*, 2017, **17**, 2235

A simple and highly sensitive spectroscopic fluorescence-detection system for multi-channel plastic-microchip electrophoresis based on side-entry laser-beam zigzag irradiation

Takashi Anazawa,*[a] Yuichi Uchiho,[a] Takahide Yokoi,[a] George Chalkidis[a] and Motohiro Yamazaki[b]

Received 25th April 2017,
Accepted 27th May 2017

DOI: 10.1039/c7lc00448f

rsc.li/loc

A five-color fluorescence-detection system for eight-channel plastic-microchip electrophoresis was developed. In the eight channels (with effective electrophoretic lengths of 10 cm), single-stranded DNA fragments were separated (with single-base resolution up to 300 bases within 10 min), and seventeen-loci STR genotyping for forensic human identification was successfully demonstrated. In the system, a side-entry laser beam is passed through the eight channels (eight A channels), with alternately arrayed seven sacrificial channels (seven B channels), by a technique called "side-entry laser-beam zigzag irradiation." Laser-induced fluorescence from the eight A channels and Raman-scattered light from the seven B channels are then simultaneously, uniformly, and spectroscopically detected, in the direction perpendicular to the channel array plane, through a transmission grating and a CCD camera. The system is therefore simple and highly sensitive. Because the microchip is fabricated by plastic-injection molding, it is inexpensive and disposable and thus suitable for actual use in various fields.

Introduction

Laser-induced-fluorescence (LIF) detection in a microfluidic channel is extensively adopted in the "lab-on-a-chip" (LOC) field due to its high sensitivity and selectivity.[1,2] Nucleic acids, proteins, cells, other biological materials, or other chemical materials are flowed or separated in the channel on the microchip. Subsequently, rare components of interest in these samples can be exclusively detected by LIF. Representative applications of LIF detection include genetic mutation testing,[3–7] short-tandem-repeat (STR) genotyping,[8–11] DNA sequencing,[12–14] immunoassay,[15–18] and flow cytometry and cell sorting.[19–22]

Additionally, multi-color and multi-channel LIF detection is very important to enhance throughput and thereby reduce time and cost for the above-mentioned applications. This is because much information about each sample is simultaneously obtained from many samples by using a single microchip. Multi-color LIF detection is widely used in genetic analysis such as STR genotyping and DNA sequencing. As for STR genotyping, for more accurate forensic human identification, up-to-18-loci multiplex PCR products from each sample are separated by electrophoresis and individually detected by up-to-five-color LIF (one color for the size standard). In DNA sequencing, DNA fragments produced by the Sanger reaction are separated by electrophoresis and detected by four-color LIF to identify their terminal base species. Systems for multi-color LIF detection conventionally adopt one of two methods: either the use of a grating to produce fluorescence spectra[9,10,12] or the use of dichroic mirrors to form split fluorescence beams of differing wavelength.[11,13,14]

Meanwhile, multi-channel LIF detection is used in a wider range of applications.[23] Three samples of PCR products (wild type or mutant rice) have been simultaneously separated and detected in a three-channel microchip.[5] Six immunoassays for ovalbumin have been simultaneously performed in an eight-channel microchip (two channels for optical alignment).[17] Moreover, as for genetic mutation testing,[7] STR genotyping,[11] and flow cytometry,[22] microchips with a larger number of channels, namely, 96 or 384, have been demonstrated. Multi-channel LIF detection using these chips was carried out by laser-beam scanning[7,11,16,17,22] or laser-beam expansion.[5,6]

In the case of the laser-beam scanning, a finely focused laser beam is scanned across the multi-channels to irradiate all the channels sequentially. Then, fluorescence from each channel is collected using a microscope objective and detected using a photomultiplier. An epi-illumination

[a] *Hitachi, Ltd., Research & Development Group, Japan.*
E-mail: takashi.anazawa.rc@hitachi.com
[b] *Hitachi High-Technologies Corporation, Science & Medical Systems Business Group, Japan*

confocal detector with a high-laser-power source is used to drastically increase the number of channels, that is, throughput.[7,11,22] In addition, four-color LIF detection using dichroic mirrors and four photomultipliers is combined with the epi-illumination confocal detection. However, the method for scanning the laser beam is complex because it requires the moving parts.

In the case of the laser-beam expansion, a laser beam is expanded to form a linear beam across the multi-channels to irradiate all the channels simultaneously. Then, fluorescence from each channel is collected using a microscope objective and simultaneously detected using a two-dimensional CCD sensor. Although this method requires no moving parts, the laser-power density (that is, fluorescence from each channel) decreases inversely with the number of channels.

In most studies, glass materials were used for the microchip. A glass microchip is preferable for highly sensitive LIF detection due to its low background noise. However, it is expensive, because photolithography and wet etching are used in its fabrication process. It is therefore not suitable for practical use. On the other hand, in other studies, plastic materials were used for the microchip.[6,9,13,14,20] A plastic microchip is inexpensive, because it is fabricated by mass-production technologies such as plastic-injection molding. It is therefore disposable and practical.

Recently, a method called "side-entry laser-beam zigzag irradiation" for multi-channel LIF detection using a plastic microchip was proposed.[24] A focused laser beam enters from the side of a multi-channel plane to pass across the channel array and simultaneously irradiate all the channels with high laser-power density. Because the cross-sectional shape of each channel is inevitably tapered due to the draft angle used in the injection-molding process, the laser beam is refracted by each channel. To overcome this deviation of the laser beam from the multi-channel plane due to laser-beam refraction by each channel, side-entry laser-beam zigzag irradiation was developed. As for this method, the A channels and B channels are arrayed alternately in a plastic microchip, with a refractive index n_C, and respectively filled with materials with refractive indexes n_A (for analysis) and n_B (for laser-beam control). The laser beam travels straight and irradiates all A channels simultaneously and effectively because the refractive actions by the A and B channels are counterbalanced by satisfying the condition $n_A < n_C < n_B$.

In this study based on side-entry laser-beam zigzag irradiation, an eight-channel plastic-microchip electrophoresis system was developed. The microchip was designed, fabricated, and evaluated in terms of the feasibility of side-entry laser-beam zigzag irradiation. Spectroscopic five-color LIF detection, by obtaining full fluorescence spectra from all eight channels at the same time, was incorporated into the system. The system successfully demonstrated simultaneous separations of a four-color allelic ladder and one-color size-standard samples for seventeen-loci STR genotyping in the eight channels. Because the system is simple, highly sensitive, and inexpensive, it is suitable for practical use.

Experimental

Microchip design and fabrication

The microchip was composed of ZEONEX (Zeon Corporation), a cycloolefin polymer, with a refractive index n_C of 1.53 at 505 nm. A multi-grooved plate was fabricated by injection molding using nickel-based alloy molds and laminated with a thin sheet (with thickness of 100 μm) by thermocompression bonding without any adhesive agent. The top of the microchip (with an outer size of 135 × 40 mm and a thickness of 1.5 mm) is shown in Fig. 1(a). Eight A channels (indicated by blue lines, numbered A-ch 1 to A-ch 8) and seven B channels (indicated by red lines, numbered B-ch 1 to B-ch 7) were alternately formed in the microchip. The microchip was placed horizontally with the thin-sheet-side facing downward. An enlarged cross-sectional design of the microchip at the laser-irradiation positions of the channels is shown in Fig. 1(b). The cross-sectional shapes of all the channels were isosceles trapezoids with an upper base length of 40 μm, a height of 40 μm, and an upper base angle of 97° (which gives a draft angle of 7°). Both legs of the trapezoids were bent slightly inward, namely, by a width of less than 2 μm, to enhance mold releasability during injection molding. All the channels around the laser-irradiation positions were arrayed parallel to each other at 200 μm intervals. As for the

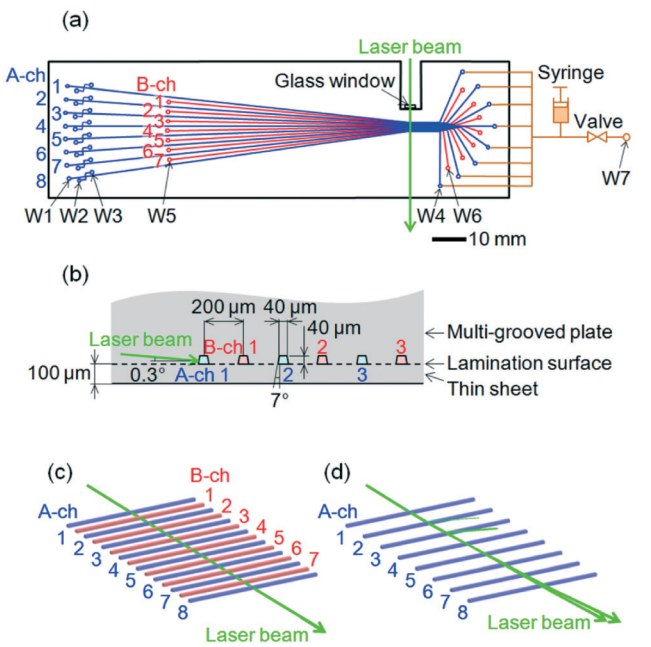

Fig. 1 Design of a multi-channel plastic-microchip. (a) Top view of the multi-channel microchip with a side-entry laser beam (green) and a polymer filling unit (brown). Eight A channels (blue, A-ch 1 to 8) for electrophoresis and seven B channels (red, B-ch 1 to 7) for laser-beam control are alternately arrayed. (b) Cross-sectional view of the multi-channel microchip of the laser-beam-irradiation region. Cross-sectional shapes of all the channels are isosceles trapezoids due to a draft angle used in plastic-injection molding. (c) Ray-trace simulation of the side-entry laser beam in the above design. (d) Ray-trace simulation of the side-entry laser beam in a design where all B channels are removed.

laser-beam's incidence, a concave portion (with a width of 6 mm and a depth of 15 mm) was formed in the microchip by milling, and a glass window was adhered to the surface of the milled end. These features were formed to suppress laser scattering in the microchip material and on the laser-beam incident surface of the microchip, respectively. Wells (with a diameter of 1.2 mm) were formed at both ends of the A channels (indicated by blue circles, W1 and W4) and the B channels (indicated by red circles, W5 and W6). Double-T cross-injectors were formed 5 mm from the W1 wells. The cross-sectional shapes of their channels and the diameters of their wells (indicated by W2 and W3) were the same as those stated above. Offsets of the double-T cross-injectors were 100 μm in length.

Inspection of the fabricated microchip

As for the fabricated microchip, the intervals between all the channels at the laser-irradiation positions were measured from the direction perpendicular to the microchip using a laser scanner. Additionally, the upper and lower surfaces of the channels were imaged using an optical microscope. Then, the upper and lower bases of the cross-sections of the channels were obtained by measuring the channel widths in the two images, respectively. The heights of the cross-sections were also obtained by measuring the relative displacement of an objective to the microchip when the two images were obtained. The upper base angles of the cross-sections were calculated from the upper and lower bases and heights of the cross-sections based on the assumption that the cross-sectional shapes are isosceles trapezoids.

The multi-channel cross-section was observed directly after the following preparation steps. First, the fabricated microchip was cut at the laser-irradiation positions (*i.e.*, across the channels) by using a plastic scoring knife. Second, the cut cross-section and the ends of the channels were embedded in epoxy resin. Third, the epoxy resin was ground to expose the cross-section. Fourth, the cross-section (with the epoxy resin in the channels) was polished and observed using an optical microscope.

Electrophoresis

A high-refractive-index liquid (HRI liquid), an uncured acrylic adhesive with a refractive index n_B of 1.66 at 505 nm, was custom-made and ordered from NTT Advanced Technology Corporation. All the B channels (W5 wells to W6 wells) were filled with the HRI liquid. Subsequently, as schematically illustrated by brown lines and symbols in Fig. 1(a) (not to scale), the W4 wells of all the A channels were connected to a polymer-filling unit, that is, a manifold composed of Teflon tubes and acrylic materials equipped with a syringe, a valve, and a common well (indicated by W7). All the A channels from the W4 wells to the W1, W2, and W3 wells were filled with POP-6™ or POP-7™ polymer solution (Applied Biosystems; refractive index n_A of 1.41 at 505 nm). A pressure of 1 MPa was applied to the polymer solution in the polymer-filling unit by pressing the piston of a syringe filled with the polymer solution with the valve closed. To increase the inner volumes of the W1, W2, and W3 wells, they were each connected to 2 mm-diameter through holes created in a 6-mm-thick acrylic plate.

A 10 μl allelic ladder sample was prepared by mixing 3 μl of AmpFlSTR® NGM SElect™ allelic ladder (Applied Biosystems), 3 μl of GeneScan™ 600 LIZ® size standard (Applied Biosystems), and 4 μl of Hi-Di™ formamide (Applied Biosystems). A 10 μl size standard sample was prepared by mixing 3 μl of GeneScan™ 600 LIZ® size standard and 7 μl of Hi-Di™ formamide. The samples were heated at 95 °C for 3 min, and then chilled on ice. Either sample was pipetted into each W2 well. The 10 μl polymer solutions were pipetted into the W1 and W3 wells. A 16 ml 1X Genetic Analyzer buffer with EDTA (Applied Biosystems) was poured into the W7 well, and the valve was opened. The solution levels of the W1, W2, W3, and W7 wells were equalized to suppress siphonic actions of the polymer solution in the A channels. The samples in the W2 wells were injected into the offsets by grounding the W1, W2, and W7 wells and applying 380 V for POP-6™ or 240 V for POP-7™ to the W3 wells for 40 s. Then, the samples in the offsets of the A channels were separated by grounding the W1 wells, applying 220 V for POP-6™ or 180 V for POP-7™ to the W2 and W3 wells, and applying 3480 V for POP-6™ or 2900 V for POP-7™ to the W7 well for 1300 s. The electric-field strengths on the A channels were 278 V cm^{-1} for POP-6™ or 232 V cm^{-1} for POP-7™. The laser-irradiation positions of the A channels were at 100 mm from the offsets; that is, the effective lengths of the A channels were 100 mm. All the electrophoresis processes were carried out at room temperature.

Laser-beam irradiation and spectroscopic fluorescence detection

As shown in Fig. 1(a), a 505 nm laser beam (Showa Optronics Co., Ltd.) was focused by a lens (with f 60 mm) and entered the side of the microchip through the glass window at a power of 15 mW. As shown in Fig. 1(b), the laser beam (with a diameter of 50 μm) irradiated A-ch 1 at an angle of 0.3° from the multi-channel plane (or the lamination surface) and perpendicularly to the axis of A-ch 1.

A perspective view of a laser-beam ray-trace simulation in the multi-channel under the above-stated conditions is shown in Fig. 1(c). As a result of applying side-entry laser-beam zigzag irradiation, the laser beam passed across the channel array and simultaneously irradiated all the channels effectively. The slightly inner bends of both legs of the trapezoidal cross-section of each channel were negligible. By contrast, a similar view when all the B channels were removed is shown in Fig. 1(d). The laser beam deviated upward from the multi-channel at A-ch 3 and irradiated only A-ch 1 and A-ch 2 effectively.

Fluorescence and scattered light beams emitted from all A and B channels were detected from below in the direction

perpendicular to the microchip. They were concurrently collimated using a camera lens (f 50 mm and F/1.4), passed through a longpass filter to cut out the laser light, passed through a transmission grating with a grating constant of 600 lines per mm, and were focused by another camera lens (f 50 mm and F/1.4) on a two-dimensional CCD sensor (Hamamatsu Photonics K.K., S7031-0908S). The direction of wavelength dispersion was perpendicular to the laser beam, that is, it is parallel to the axes of the channels.

For multi-channel spectroscopic imaging, instead of using POP-6™ or POP-7™ polymer solution, 70% formamide aqueous solution (70% FA) with the same refractive index of n_A = 1.41 or 70% FA containing 100 nM dR110 dye-labeled C primers or 100 nM dROX dye-labeled T primers prepared from an ABI Prism BigDye Primer Cycle Sequencing Ready Reaction Kit (Applied Biosystems) was injected into all the A channels. Full spectral images were captured by the CCD sensor at an exposure time of 200 ms. For electrophoresis, partial images of the eight A channels were continuously acquired for an exposure time of 100 ms.

Results and discussion

Fabricated microchip

The photographs of the fabricated microchip are shown in Fig. 2: (a) shows a top view of the eight A channels and the seven B channels around the laser-irradiation positions; (b) shows the cross-sections of B-ch 5 and A-ch 6 at the laser-irradiation positions. The intervals of the channels were 200.4 ± 1.0 μm (average ± standard deviation for n = 3 (microchips) × 14 (intervals) = 42 data). The upper bases, lower bases, and heights of the cross-sections were 39.1 ± 0.3 μm, 49.2 ± 0.2 μm, and 39.4 ± 0.1 mm (average ± standard deviation for n = 3 (microchips) × 15 (channels) = 45 data), respectively. The upper-base angles of the cross-sections were therefore 7.27 ± 0.22°. These results show that the fabricated microchip accurately complies with the design shown in Fig. 1(b). Laser-beam ray-trace simulations revealed that (i) variation in the upper-base angles of the cross-sections is the most serious factor degrading side-entry laser-beam zigzag irradiation and (ii) the standard deviation should be less than 1° to achieve irradiation. Such small differences between the actual values and the designed values, therefore, did not degrade the irradiation. The slightly inner bends of both legs of the isosceles trapezoids can be observed in Fig. 2(b). They greatly improved the reproducibility of the cross-sectional shapes of the channels. The lamination surface between the multi-grooved plate and the thin sheet (with a thickness of 100 μm) can also be observed, although the plate and sheet are almost optically homogeneous. The microchip on a horizontal optical stage, equipped with the polymer-filling unit and irradiated by the side-entry laser beam, is shown in Fig. 2(c). A green laser beam can be observed in the microchip. Multi-channel spectroscopic fluorescence was detected from underneath the optical stage.

Detection of multi-channel background-light and fluorescence spectra

A multi-channel spectral image of linear background light along the laser beam in the microchip when the A and B channels were respectively filled with 70% FA and the HRI

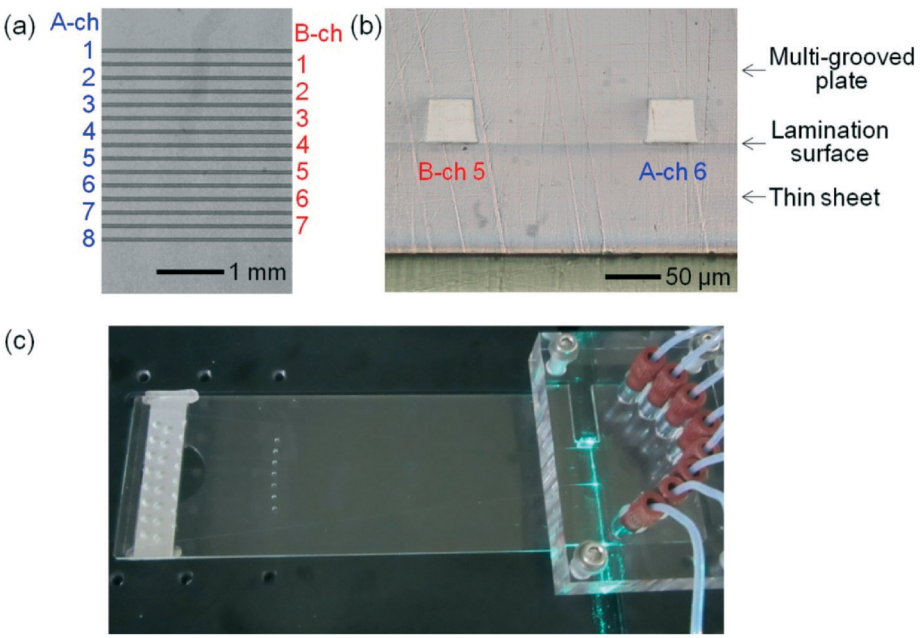

Fig. 2 Photographs of the fabricated multi-channel microchip. (a) Top view of the microchip around the laser-irradiation region showing eight A channels and seven B channels. (b) Cross-sectional view of the microchip around the laser-irradiation region showing B-ch 5 and A-ch 6. (c) The microchip on an optical stage with the side-entry laser beam and the polymer filling unit.

liquid is shown in Fig. 3(a) (on a gray scale of 50 to 3000). 70% FA was used instead of the polymer solution because it easily fills all the A channels with constant dye concentration, as shown in Fig. 3(c), because the viscosity of 70% FA is much lower than that of the polymer solution. The horizontal axis indicates the position in the laser-beam direction (*i.e.*, channel-array direction) and the vertical axis indicates the wavelength. The image includes the background-light spectra of all the A and B channels indicated in Fig. 3(a). Such multi-channel spectra were obtained for the first time thanks to the system combining side-entry laser-beam zigzag irradiation and simultaneous spectroscopic fluorescence detection with the multi-channel microchip.

A horizontal, zonal, and strong signal around 592 nm across the image, as indicated by RS1 in Fig. 3(a), was obtained from the Raman-scattered light generated by exciting the microchip material, or the cycloolefin polymer, with the laser beam at 505 nm. By Raman spectroscopic analysis of the cycloolefin polymer, a strong intensity Raman peak between 2836–2961 cm^{-1} was observed and attributed to the signal. As shown in an enlarged view (including B-ch 6, A-ch 7, B-ch 7, and A-ch 8) on a gray scale of 1500 to 3000 in Fig. 3(a), the intensity of the signal at 592 nm is weaker at the A and B channel positions than at the other positions. This is because the cycloolefin polymer is not present in the A and B channels; however, the laser beam slightly irradiates the cycloolefin polymer above and below the channels because the laser-beam diameter (50 μm) is slightly larger than the channel depths (40 μm). Similarly, horizontal, zonal, but smaller signals around 534–546 nm seen across the image were also obtained from Raman light-scattering of the cycloolefin polymer. These Raman light-scattering signals are unavoidable when any kind of plastic is used as the material of the microchip. However, as for the developed system, it is possible to reduce their influence on fluorescence detection by using a fluorescence signal in a spectral region that does not overlap with the Raman light-scattering spectra.

On the other hand, strong spot signals at 535 and 550 nm on the B channels, as indicated by RS2 in Fig. 3(a), were obtained from the Raman-scattered light generated by exciting the HRI liquid with the laser beam at 505 nm. A uniform intensity of Raman light-scattering signals at 535 and 550 nm was obtained from all the B channels. These results provide direct evidence that the laser beam is equally transmitted in all the B channels, because strong Raman light-scattering signals at 535 and 550 nm were obtained only on the B channels, that is, the positions where the HRI liquid is present. The intensity distribution of background light along the channel array at 550 nm is shown in Fig. 3(b) on a vertical scale of 50 to 3000. The coefficient of variation (CV) of intensities of the Raman light-scattering signals (indicated by closed arrow heads) of all the B channels was only 9%. It is also evident that the laser beam is equally transmitted in all the A channels as well as all the B channels because it is impossible for the laser beam to be transmitted in all the B channels but not in all the A channels. Consequently, these

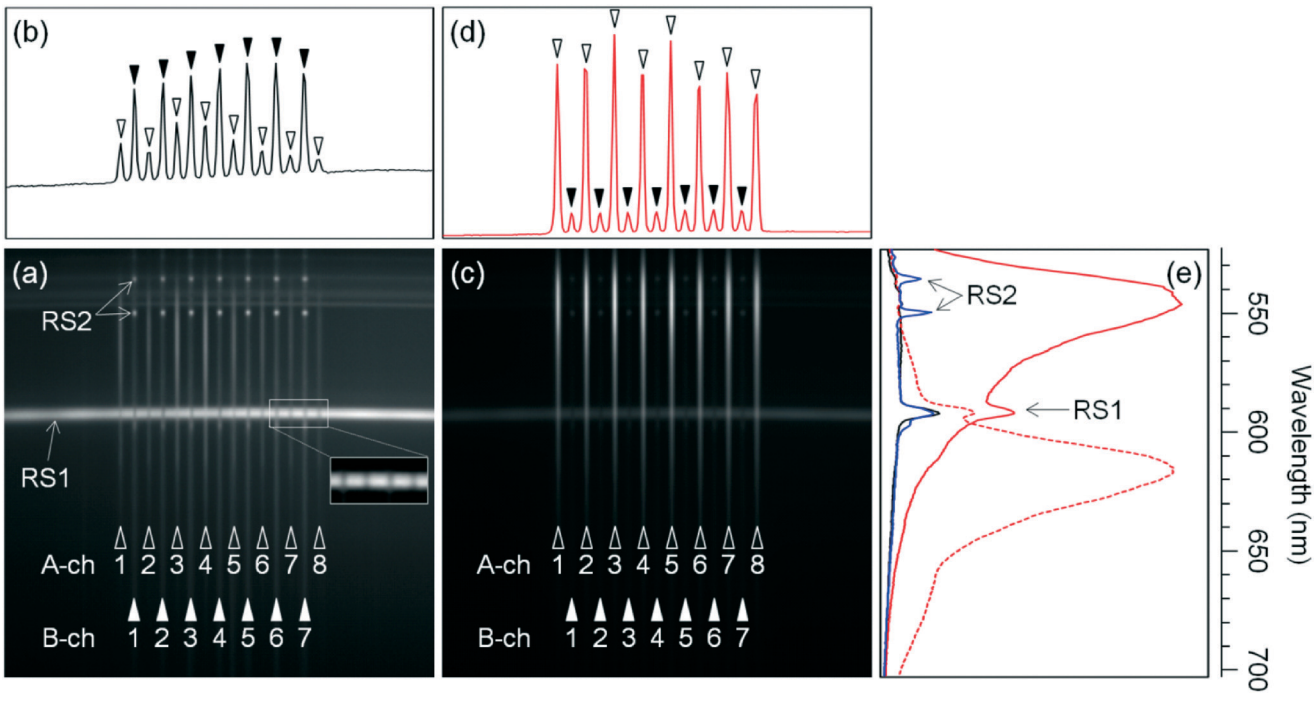

Fig. 3 Multi-channel spectral images. (a) Multi-channel background-light spectral image (gray scale: 50–3000). (b) Intensity distribution of background light along the channel array at 550 nm (vertical scale: 50–3000). (c) Multi-channel dR110 fluorescence spectral image (gray scale: 500–12 000). (d) Intensity distribution of dR110 fluorescence along the channel array at 550 nm (vertical scale: 500–12 000). (e) Spectra of dR110 fluorescence (red solid line), background light (black line), and dROX fluorescence (red dashed line) on A-ch 5, and background light (blue line) on B-ch 5 (horizontal scale: 500–12 000).

results show that the laser beam effectively irradiated all the A and B channels by side-entry laser-beam zigzag irradiation. Conversely, even before injecting a fluorescent sample into the A channels, it is possible to finely adjust the laser-beam position relative to the multi-channel so that a uniform intensity of Raman-scattered light beams at 535 and 550 nm is obtained from all the B channels; that is, the side-entry laser-beam zigzag irradiation works well.

A multi-channel spectral image where the A-channel fillings were replaced with 70% FA containing 100 nM dR110 is shown in Fig. 3(c) (on a gray scale of 500 to 12 000). Note that the gray scale in Fig. 3(c) is different from that in Fig. 3(a). The image includes the fluorescence spectra of all A channels, and the background light spectra of all B channels, as indicated in Fig. 3(c).

Intensity distributions of fluorescence of dR110 (λ_{max} = 546 nm) and background light along the channel array at 550 nm are shown in Fig. 3(d) (on a vertical scale of 500 to 12 000). The intensities of the A channels (indicated by open arrow heads) drastically increased compared to those in Fig. 3(b), whereas the intensities of the B channels (indicated by closed arrow heads) did not change compared to those in Fig. 3(b). A uniform fluorescence intensity of all the A channels (with a CV of only 12%) was obtained. This result is consistent with the uniform intensity of the Raman light-scattering signals of all the B channels; that is, the laser beam simultaneously and effectively irradiated all the A and B channels by side-entry laser-beam zigzag irradiation. As for three different microchips examined for different days, the CVs of intensities of Raman light-scattering signals at 550 nm of all the B channels were 13%, 12%, and 12% respectively. It is therefore concluded that the repeatability of the side-entry laser-beam zigzag irradiation is high.

The spectra of dR110 (λ_{max} = 546 nm) fluorescence and background light on A-ch 5 are shown as red and black solid lines, respectively, in Fig. 3(e) (on a horizontal scale of 500 to 12 000). The spectrum of the background light on B-ch 5 is shown as a blue solid line. On the other hand, when the A-channel fillings were replaced with 70% FA containing 100 nM dROX, the fluorescence spectrum of dROX (λ_{max} = 616 nm) on A-ch 5 is shown as a red dashed line in Fig. 3(e). Although the fluorescence spectra in the figure include the background-light spectrum, respectively, they agree well with the fluorescence spectra of dR110 and dROX reported in the literature, respectively. Here, small peaks at 592 nm in the fluorescence spectra and the background-light spectrum of A-ch 5, and the background-light spectrum of B-ch 5, as indicated by RS1 in Fig. 3(e), were obtained from the Raman-scattered light of the cycloolefin polymer. Small peaks at 535 and 550 nm in the background spectrum of B-ch 5, as indicated by RS2 in Fig. 3(e), were obtained from the Raman-scattered light of the HRI liquid.

According to the results from the analysis of time courses of fluorescence intensities in the ranges 540–550 and 610–620 nm, the lower detection limits (concentrations) of fluorescence of dR110 and dROX were 42 and 22 pM, respectively.[24] On the other hand, 100 nM dR110 and dROX is detectable without CCD-sensor saturation, as shown in Fig. 3(e). The fluorescence-detection dynamic range is therefore more than three orders of magnitude. These results indicate that it is possible to obtain any fluorescence spectrum with high sensitivity and a high dynamic range in a range of 530–700 nm for all the A channels simultaneously and independently. In fact, as shown in Fig. 5, other than dR110 and dROX, five fluorescence spectra, namely, those of 6-FAM (λ_{max} = 522 nm), VIC (λ_{max} = 554 nm), NED (λ_{max} = 575 nm), PET (λ_{max} = 595 nm), and LIZ (λ_{max} = 655 nm), were detected simultaneously.

Multi-channel microchip electrophoresis

The digital-electrophoresis images of the eight A channels are shown in Fig. 4. In all the A channels filled with POP-7™, the size standard samples, that is, the single-stranded DNA fragments labeled with one color dye, LIZ (λ_{max} = 655 nm), were electrophoresed. The time course of fluorescence intensity in the range of 650–660 nm of each A channel was used to create each image. Uniform, high-speed, and high-resolution separations in all the A channels were achieved. The single-stranded DNA fragments were separated with a single-base resolution up to 300 bases within 10 min. The CV

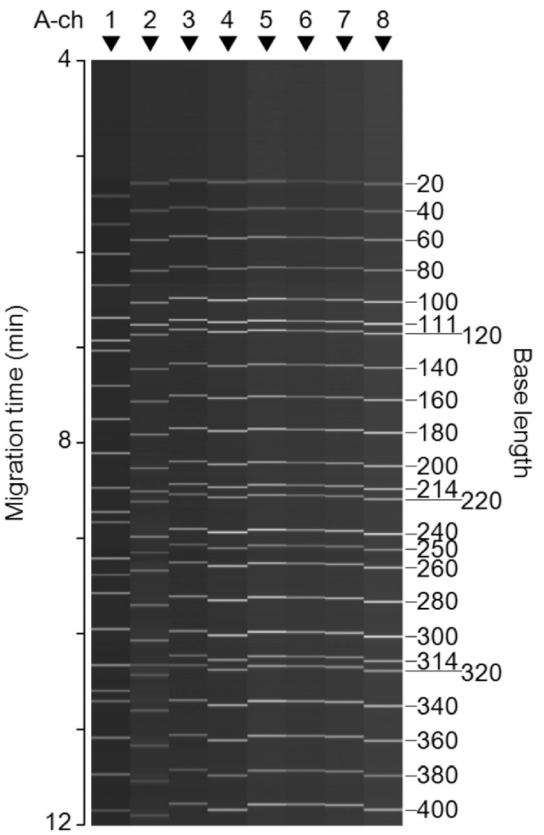

Fig. 4 Obtained digital-electrophoresis images of the eight A channels, where GeneScan™ 600 LIZ size standard samples (single-stranded DNA fragments) are separated at a single-base resolution.

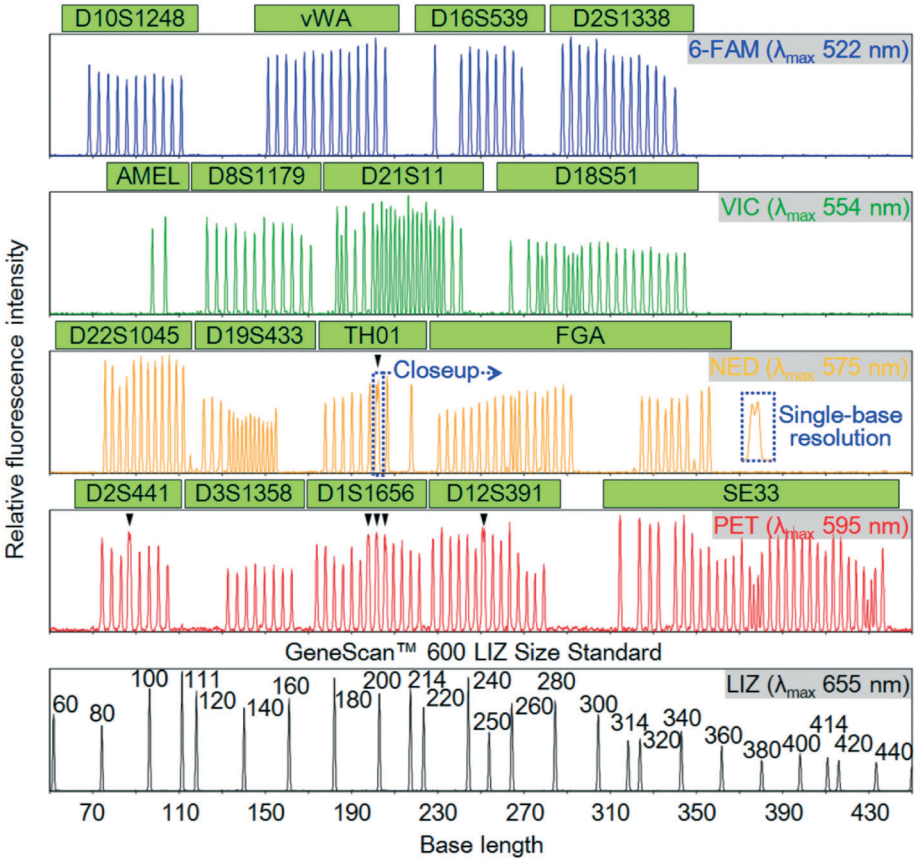

Fig. 5 Representative electrophoretic separation of AmpFlSTR® NGM SElect™ allelic ladder for 17 STR loci forensic genotyping. Single-stranded DNA fragments labeled with five colors (6-FAM, VIC, NED, PET, and LIZ) migrating in each A channel were simultaneously detected.

of migration time of each DNA fragment for the eight A channels was small (1%). Third-order approximation of migration time and base length in each A channel makes it possible to identify the base length of any DNA fragments in the range of 200 to 400 bases with an accuracy of less than one base. By adopting a temperature controller for the microchips during electrophoresis, it will be possible to improve both the CV of migration time and accuracy of base-length identification. On the other hand, the CV of fluorescence intensity of each DNA fragment in the eight A channels was 26%. This value is larger than the CV of fluorescence intensities shown in Fig. 3(d), namely, 12%, because the concentration of the sample injected into the offsets of the A channels is variable.

A representative electrophoretic separation of the Allelic Ladder sample obtained within 19 min in an A channel filled with POP-6™ is shown in Fig. 5. Single-stranded DNA fragments in the allelic ladder sample were labeled with any one of the five color dyes, 6-FAM (λ_{max} = 522 nm), VIC (λ_{max} = 554 nm), NED (λ_{max} = 575 nm), PET (λ_{max} = 595 nm), or LIZ (λ_{max} = 655 nm) to realize the detection of seventeen STR loci, or a total of 256 alleles, at the same time. The time course of the full fluorescence spectrum in the range of 530–700 nm was used to deconvolute the spectral overlaps between the five colors. As shown in Fig. 5, their deconvolution gave the time course of fluorescence intensity of each color dye corresponding to the concentration of each one. Here, the horizontal axis is converted from time to base length on the basis of the electrophoretic separation of the LIZ size-standard shown in the figure. All the allelic peaks in the other four electrophoretic separations are detected with a high signal-to-noise ratio. It is easy to identify almost all the allelic peaks differing in length by four bases, two bases, or a single base. Six pairs of double allelic peaks differing in length by a single base are indicated by arrow heads in the figure. Alleles 9.3 and 10 of TH01 in the NED electrophoretic separation are resolved, as shown in the close up in the figure. Alleles 11.3 and 12 of D2S441 and alleles 19.3 and 20 of D12S391 in the PET electrophoretic separation are also resolved. On the other hand, only alleles 14.3 and 15, alleles 15.3 and 16, and alleles 16.3 and 17 of D1S1656 in the PET electrophoretic separation are not sufficiently resolved. However, it is possible to slightly optimize the electrophoretic conditions to resolve all the allelic peaks because single-base resolution is obtained at least in the region of 40–320 bases under the electrophoretic conditions.

Similar electrophoretic separation of the allelic ladder sample to that shown in Fig. 5 was also obtained in the other seven A channels on the same multi-channel microchip. It is therefore possible to apply multi-channel microchip electrophoresis using the developed spectroscopic fluorescence-

detection system (combining side-entry laser-beam zigzag irradiation and spectroscopic fluorescence detection) for high-throughput and rapid forensic human identification by multiplex STR loci genotyping.

Conclusion

A simple, highly sensitive, multi-color, and multi-channel fluorescence detection system was developed for multi-channel microchip electrophoresis by side-entry laser-beam zigzag irradiation. The system successfully demonstrated seventeen-loci STR genotyping (for forensic human identification) with five-color and eight-channel fluorescence detection. It is easy to apply the system to other analyses such as DNA sequencing. Because the microchip is fabricated by plastic-injection molding, it is inexpensive and disposable; therefore, it is suitable for actual use in various fields.

It is, however, possible to improve the system in some aspects. The number of A channels can be increased depending on its applications. The laser-beam ray-trace simulation revealed that, for example, twenty-four A channels and twenty-three B channels are simultaneously and effectively irradiated by a side-entry laser beam. The laser-beam-irradiation efficiency relative to A-ch 1 slightly decreases with increasing channel number (due to a laser-beam-reflection loss at each channel), but it is still relatively high at A-ch 8 (94%), A-ch 16 (90%), and A-ch 24 (85%).

In the A channels, it is also possible to use any liquid with a refractive index other than n_A of 1.41. The laser-beam ray-trace simulation also revealed that, for example, the A channels filled with water (with refractive index n_A of 1.33) and the B channels filled with a liquid or solid material with a higher refractive index (n_B of 1.73) are simultaneously and effectively irradiated by a side-entry laser beam, because the refractive actions by the A and B channels are counterbalanced.[24] Such a higher-refractive-index material is stably manufacturable.

Moreover, it is possible to integrate sample-preparation functions on the multi-channel microchip.[9,10,16–18] Such sample-to-answer systems will enhance actual use of microchip-based analysis, or LOC.

Acknowledgements

We thank Chihiro Uematsu and Dr. Kenichi Takeda of Hitachi, Ltd. for their valuable discussions on the manuscript. We also thank Takehiko Shibasaki and Yoshitaka Kodama of Hitachi High-Technologies Corporation for the facilitation of this research.

References

1 H. Gai, Y. Li and E. S. Yeung, *Top. Curr. Chem.*, 2011, **304**, 171–201.
2 M. E. Johnson and J. P. Landers, *Electrophoresis*, 2004, **25**, 3513–3527.
3 H. Zhang, J. Song, H. Ren, Z. Xu, X. Wang, L. Shan and J. Fang, *PLoS One*, 2013, **8**, e54510.
4 J. Y. Choi, Y. T. Kim, J. Ahn, K. S. Kim, D. G. Gweon and T. S. Seo, *Biosens. Bioelectron.*, 2012, **35**, 327–334.
5 H. Nan, S. W. Lee and S. H. Kang, *Talanta*, 2012, **97**, 249–255.
6 F. Dang, O. Tabata, M. Kurokawa, A. A. Ewis, L. Zhang, Y. Yamaoka, S. Shinohara, Y. Shinohara, M. Ishikawa and Y. Baba, *Anal. Chem.*, 2005, **77**, 2140–2146.
7 C. A. Emrich, H. Tian, I. L. Medintz and R. A. Mathies, *Anal. Chem.*, 2002, **74**, 5076–5083.
8 Y. T. Kim, H. Y. Heo, S. H. Oh, S. H. Lee, H. Kim Do and T. S. Seo, *Electrophoresis*, 2015, **36**, 1728–1737.
9 D. Le Roux, B. E. Root, C. R. Reedy, J. A. Hickey, O. N. Scott, J. M. Bienvenue, J. P. Landers, L. Chassagne and P. de Mazancourt, *Anal. Chem.*, 2014, **86**, 8192–8199.
10 A. J. Hopwood, C. Hurth, J. Yang, Z. Cai, N. Moran, J. G. Lee-Edghill, A. Nordquist, R. Lenigk, M. D. Estes, J. P. Haley, C. R. McAlister, X. Chen, C. Brooks, S. Smith, K. Elliott, P. Koumi, F. Zenhausern and G. Tully, *Anal. Chem.*, 2010, **82**, 6991–6999.
11 J. R. Scherer, P. Liu and R. A. Mathies, *Rev. Sci. Instrum.*, 2010, **81**, 113105.
12 C. P. Fredlake, D. G. Hert, C. W. Kan, T. N. Chiesl, B. E. Root, R. E. Forster and A. E. Barron, *Proc. Natl. Acad. Sci. U. S. A.*, 2008, **105**, 476–481.
13 Y. Shi, *Electrophoresis*, 2006, **27**, 3703–3711.
14 Y. Shi and R. C. Anderson, *Electrophoresis*, 2003, **24**, 3371–3377.
15 Y. Huang, S. Zhao, M. Shi and H. Liang, *Analyst*, 2011, **136**, 2119–2124.
16 J. Kong, L. Jiang, X. Su, J. Qin, Y. Du and B. Lin, *Lab Chip*, 2009, **9**, 1541–1547.
17 S. B. Cheng, C. D. Skinner, J. Taylor, S. Attiya, W. E. Lee, G. Picelli and D. J. Harrison, *Anal. Chem.*, 2001, **73**, 1472–1479.
18 D. S. Reichmuth, S. K. Wang, L. M. Barrett, D. J. Throckmorton, W. Einfeld and A. K. Singh, *Lab Chip*, 2008, **8**, 1319–1324.
19 M. E. Piyasena and S. W. Graves, *Lab Chip*, 2014, **14**, 1044–1059.
20 H. Shang, K. A. Hyun, M. H. Kwon, K. S. Ha, C. Joo and H. I. Jung, *Electrophoresis*, 2013, **34**, 3103–3110.
21 M. J. Kim, S. C. Lee, S. Pal, E. Han and J. M. Song, *Lab Chip*, 2011, **11**, 104–114.
22 B. K. McKenna, A. A. Selim, F. Richard Bringhurst and D. J. Ehrlich, *Lab Chip*, 2009, **9**, 305–310.
23 J. F. Dishinger and R. T. Kennedy, *Electrophoresis*, 2008, **29**, 3296–3305.
24 T. Anazawa, T. Yokoi and Y. Uchiho, *Anal. Chem.*, 2015, **87**, 8623–8628.

